Advanced Composite Materials
Publication details, including instructions for authors and subscription information:
http://www.tandfonline.com/loi/tacm20

Finite element analysis of FRP tube assemblies for bridge decks

Yuelin Shen , Minjie Xu , K. Chandrashekhara & Antonio Nanni

Version of record first published: 02 Apr 2012.

To cite this article: Yuelin Shen , Minjie Xu , K. Chandrashekhara & Antonio Nanni (2002): Finite element analysis of FRP tube assemblies for bridge decks , Advanced Composite Materials, 11:2, 151-169

To link to this article: http://dx.doi.org/10.1163/156855102760410342

Adv. Composite Mater., Vol. 11, No. 2, pp. 151–169 (2002)

Also available online - www.vsppub.com

Finite element analysis of FRP tube assemblies for bridge decks

YUELIN SHEN [1], MINJIE XU [1], K. CHANDRASHEKHARA [1,*] and ANTONIO NANNI [2]

[1] *Department of Mechanical and Aerospace Engineering and Engineering Mechanics, University of Missouri-Rolla, Rolla, MO 65409, USA*
[2] *Department of Civil Engineering, Center for Infrastructure Engineering Studies, University of Missouri-Rolla, Rolla, MO 65409, USA*

Received 31 October 2001; accepted 17 April 2002

Abstract—Fiber reinforced polymer (FRP) composite materials have many advantages over traditional building materials. They are becoming more and more popular in civil engineering applications. FRP pultruded tubes are easy to fabricate and can be easily assembled for different applications. In this paper, FRP tube assemblies of variable size, fiber material, tube wall thickness, and different installation are studied using finite element analysis. The deflection and stress distribution are listed for each case. When compared to experimental results, the numerical analysis shows good correlation. Data gained in this study can be used for design and optimization of FRP tube assemblies for bridge deck construction and similar applications in civil engineering.

Keywords: Bridge deck; composite materials; fiber reinforced polymer (FRP); finite element analysis; pultrusion; tube assembly.

1. INTRODUCTION

Fiber reinforced polymer (FRP) composite materials have many advantages over traditional construction materials such as steel and reinforced concrete. These advantages include lightweight, resistance to environmental damage, long life, automated fabrication and rapid installation. FRP composites are gaining more and more popularity in construction. They have been used in demonstration projects to build bridges and residential buildings [1, 2] and have been the focus of studies in designing and manufacturing [3–5]. Compared with other FRP fabrication methods, the pultrusion process is fast and suitable for large-scale production. In

*To whom correspondence should be addressed.

particular, pultruded FRP tubes are easy to assemble to form a structural subsystem for civil engineering applications.

Two most widely used reinforcements in FRP are carbon fiber and glass fiber. Carbon fiber reinforced polymer (CFRP) composites are much stiffer than glass fiber reinforced polymer (GFRP) composites, but CFRP composites are also more expensive. The material properties as well as the cost must be taken into consideration for use of FRP in construction. It is profitable to use both GFRP and CFRP tubes in the tube assembly to meet certain stiffness requirements that cannot be satisfied by using GFRP only. This is the philosophy adopted in the designing of the tube assembly in this paper.

Finite element analysis (FEA) has been successfully used to study the deflection and stress distributions of a loaded structure [6, 7]. In this paper, FRP tube assemblies of variable configurations are analyzed. These configurations include geometry, fiber material, tube layout pattern, and installation. The results can be used to optimize the design of FRP bridge decks and similar structures. ABAQUS commercial finite element analysis code is used for the numerical analysis. Three case studies are investigated to compare the results from ABAQUS with the results from analytical studies and experiments. The modeling is discussed and the results for different tube assemblies are presented. Finally, a case study of a four-layer bridge deck is conducted to demonstrate the practicality of this work.

The relevance of this paper is in the numerical validation and interpretation of the experimental results obtained from the flexural tests conducted in the laboratory. In particular, FEA allows the engineer to predict the performance of complex built-up members and identify the critical regions. Ultimately, FEA becomes one of the necessary tools in the design process for structural optimization.

2. ANALYSIS OF FRP TUBES

ABAQUS finite element code can be used in various areas such as solid mechanics, heat transfer, and fluid mechanics, and is suitable for the analysis of composite structures. Before complex tube assemblies are analyzed, the available results from literature are used to validate the ABAQUS finite element model. In this study, shell element S4R [8] is used. It is a general-purpose 4-node shell element using reduced integration. Since transverse shear effect has been considered in this element, it can be used to model both thin and thick structures.

2.1. Cantilever box beam bending

Several studies have been made on the composite box beam [9–11]. The composite cantilever beam with set up shown in Fig. 1 was given as an example in Bank *et al.* [9] and is chosen to verify the results from ABAQUS.

A 39.370 in (1000 mm) long cantilever box beam is loaded at its free end by a concentrated force of 22.47 lb (100 N). The composite tube, with wall thickness

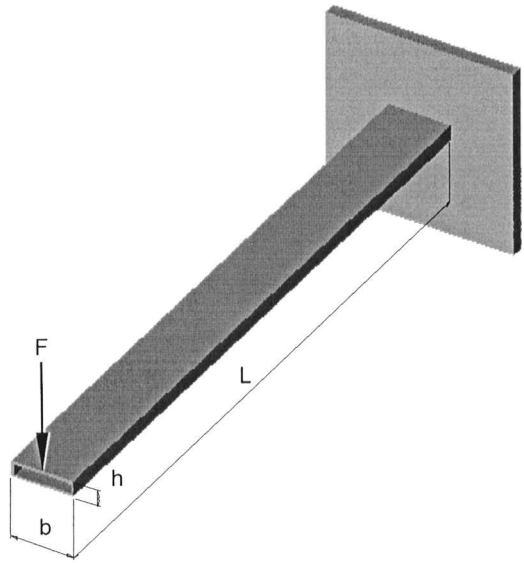

Figure 1. Geometry of cantilever beam.

Table 1.
Deflection of the cantilever box beam at the free end

Cross-section	Deflection (in) [9]	Deflection (in) using ABAQUS
$b = 3.94$ in, $h = 0.98$ in	0.2375	0.2372
$b = 0.98$ in, $h = 3.94$ in	0.0278	0.0275

Note: 1 in = 25.4 mm.

$t = 0.039$ in (1 mm), has a rectangular cross-section. Two different cases are compared, one with $b = 3.937$ in (100 mm), $h = 0.984$ in (25 mm) and the other with $b = 0.984$ in (25 mm), $h = 3.937$ in (100 mm). The material is graphite/epoxy T300/5208. Its properties are $E_{\mathrm{L}} = 26\,245$ psi (181.0 GPa), $E_{\mathrm{T}} = 1885$ psi (13.0 GPa), $\nu_{\mathrm{LT}} = 0.28$, $G_{\mathrm{LT}} = 1040$ psi (7.17 GPa) (L represents the fiber direction and T represents the transverse direction). The FEA results are compared with analytical solutions of Bank *et al.* [9] and are listed in Table 1. The correlation is very good.

2.2. Bending of a single tube

A simply supported FRP tube subjected to bending is analyzed and compared with an experiment. The test setup is shown in Fig. 2 with the following dimensions: $L = 96$ in (2438 mm), $l = 84$ in (2133 mm), $d = 12$ in (304.8 mm), $a = 3$ in (76.2 mm), $t = 0.25$ in (6.35 mm). The tube material is glass/epoxy with properties obtained from coupon tests: $E_{\mathrm{L}} = 3500$ psi (24.138 GPa), $E_{\mathrm{T}} = 1200$ psi (8.276 GPa), $\nu_{\mathrm{LT}} = 0.26$, $G_{\mathrm{LT}} = 600$ psi (4.138 GPa). These properties are used

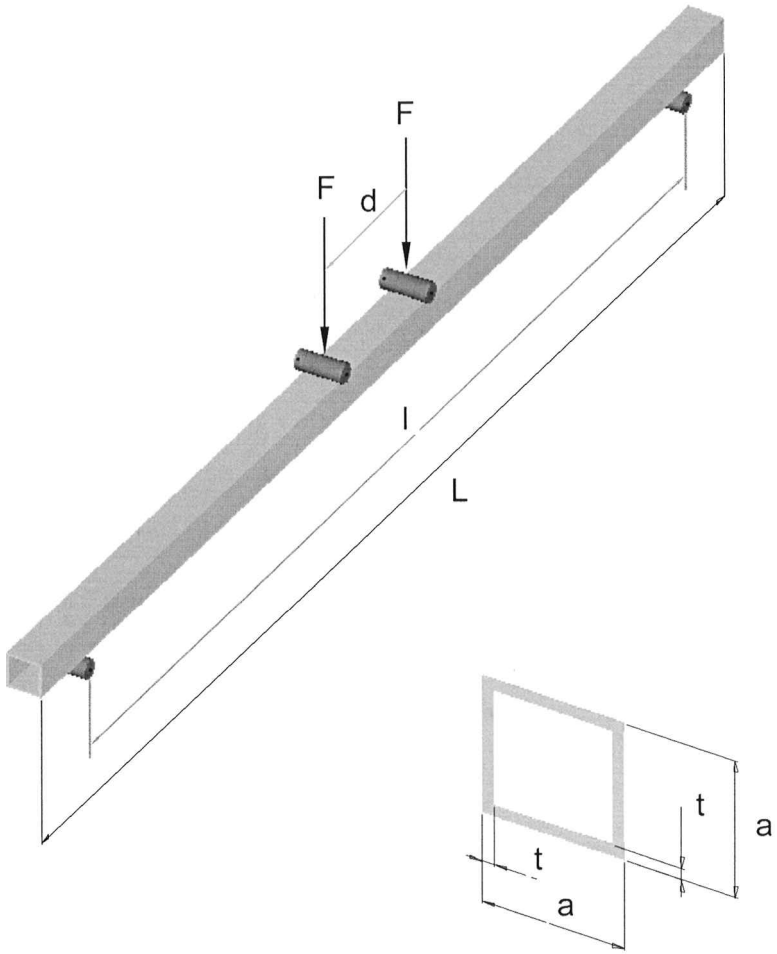

Figure 2. Single tube bending test model.

in the ABAQUS model. The finite element results compared with the experimental results are shown in Fig. 3.

Figure 3a shows the comparison of mid-span deflection. The experimental curve is an envelope obtained from cycles of loading and unloading. In the experiment, the load increases quasi-statically. When the tube breaks, the load reaches 5200 lb (23 140 N) and the maximum deflection is 5.4 in (137.2 mm). The tube deforms linearly throughout the loading history. The details of the experimental work have been reported in our earlier study [12]. The straight bold line represents the result from ABAQUS using linear static analysis. When the load is 5200 lb (23 140 N), the deflection is 5.0 in (127.0 mm). Figure 3b provides the comparison of the strain measured at the bottom of the mid-span section. The final strain reaches 0.0113 in/in in the experiment and is in good agreement with the numerical results.

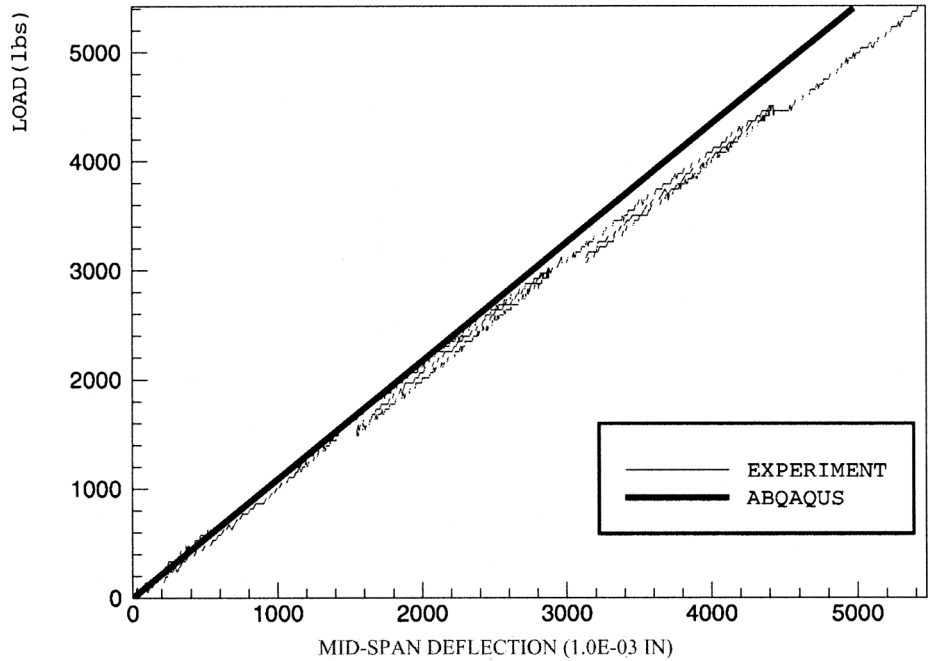

(a) Load *vs.* deflection

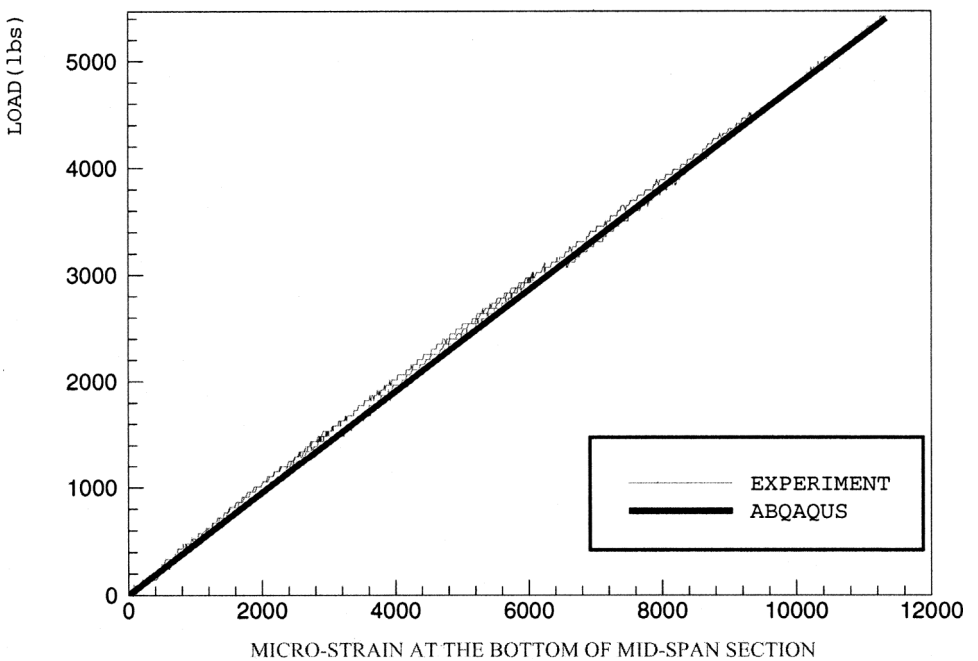

(b) Load *vs.* strain

Note: 1 in = 25.4 mm, 1 lb = 4.45 N

Figure 3. Single tube bending test results.

3. ANALYSIS OF FRP TUBE ASSEMBLY

Two tubes glued together (Fig. 4) and an assembly of four layers of tubes glued together (Fig. 5) are analyzed and the results are compared with the experiments. The material properties and the geometry of the individual tube are those presented in the previous section. For the numerical analysis, the tubes in the assemblies are assumed to be perfectly bonded. Figure 6a is the comparison of load-deflection curve for the two-tube assembly. In the experiment, there is no apparent slip at the glued interface and this confirms the assumption of perfect bonding. The two-tube assembly breaks at a section near the loading knife under a load of 14 000 lb (62 300 N). Throughout the loading history, the assembly behaves linearly and the load *vs*. deflection curve is a straight line. Figure 6b is the comparison of strain measured at the bottom of the mid-span section. The strain from the numerical analysis has good correlation with the experimental value.

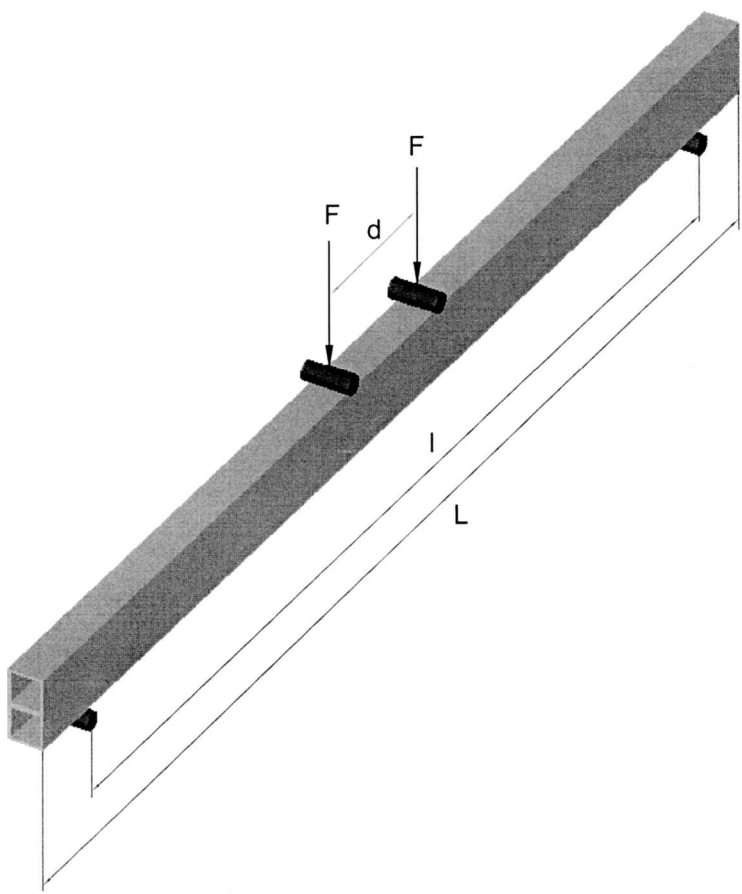

Figure 4. Two-tube assembly bending test model.

Figure 7a compares FEA and experimental load–deflection curves of the four-layer tube assembly. In the experiment, the four-layer tube assembly deforms almost linearly up to a load of approximately 12 000 lb (53 400 N). When the load exceeds 12 000 lb (53 400 N), the cross-section of the tubes in the third layer changes from

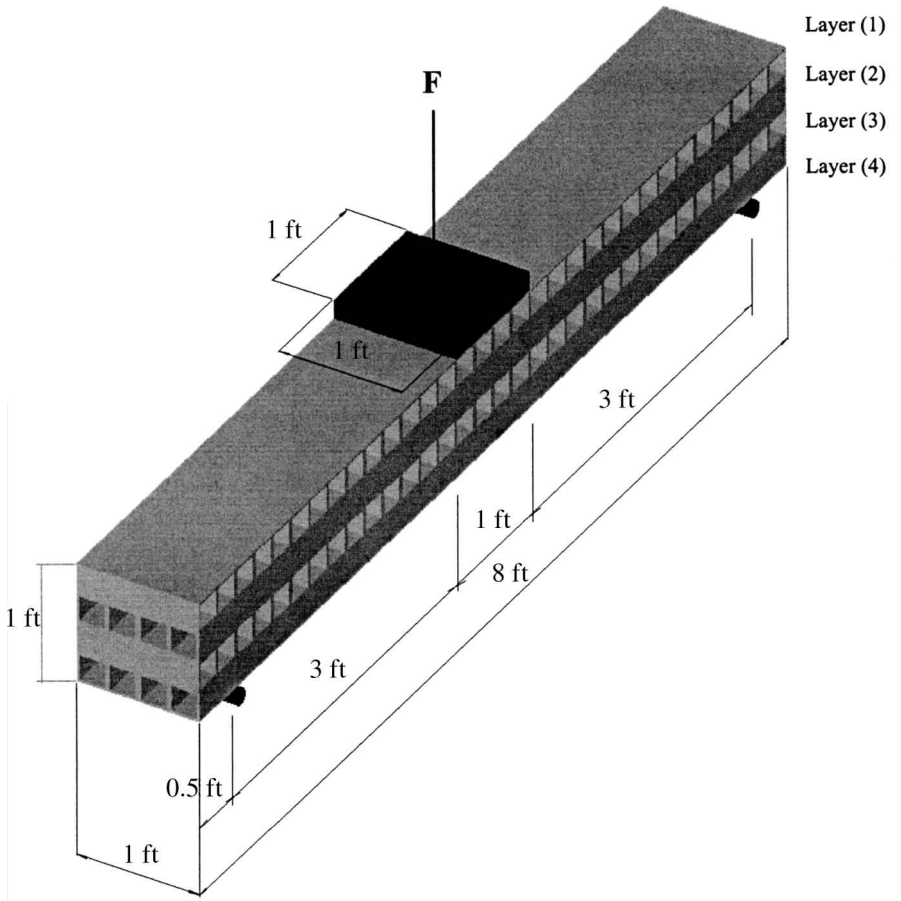

(a) Geometry of four-layer tube assembly

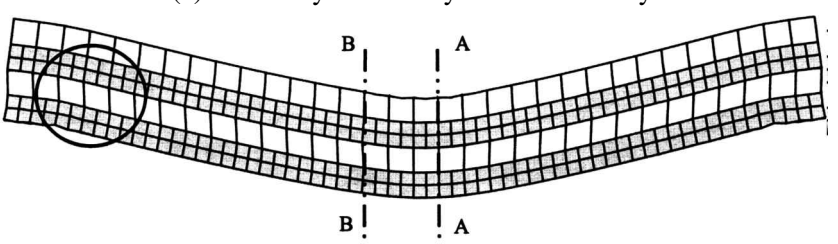

(b) Deformed shape

Note: 1 ft = 12 in, 1 in = 25.4 mm

Figure 5. Four-layer tube assembly bending test model.

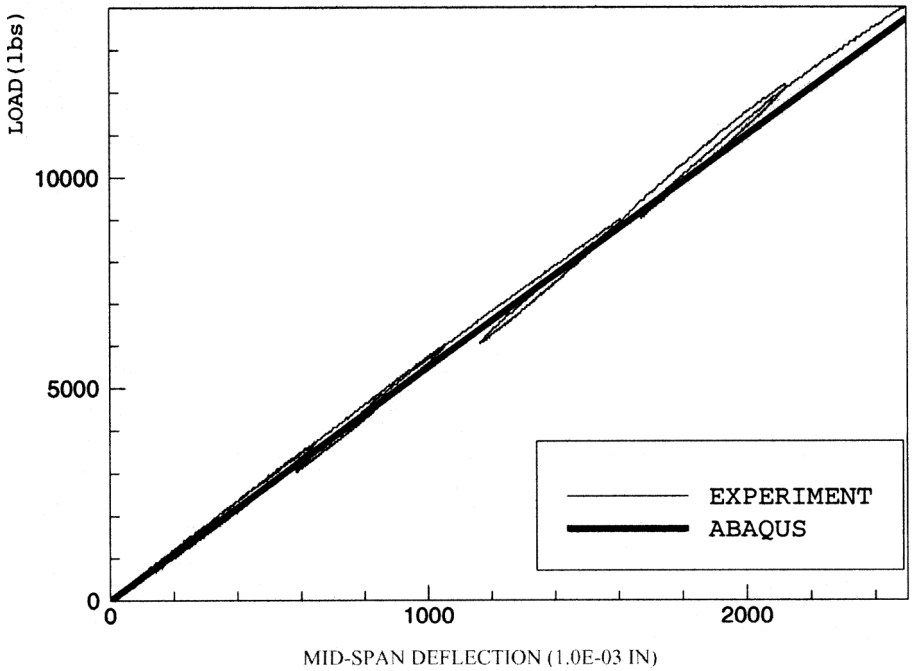

(a) Load *vs.* deflection

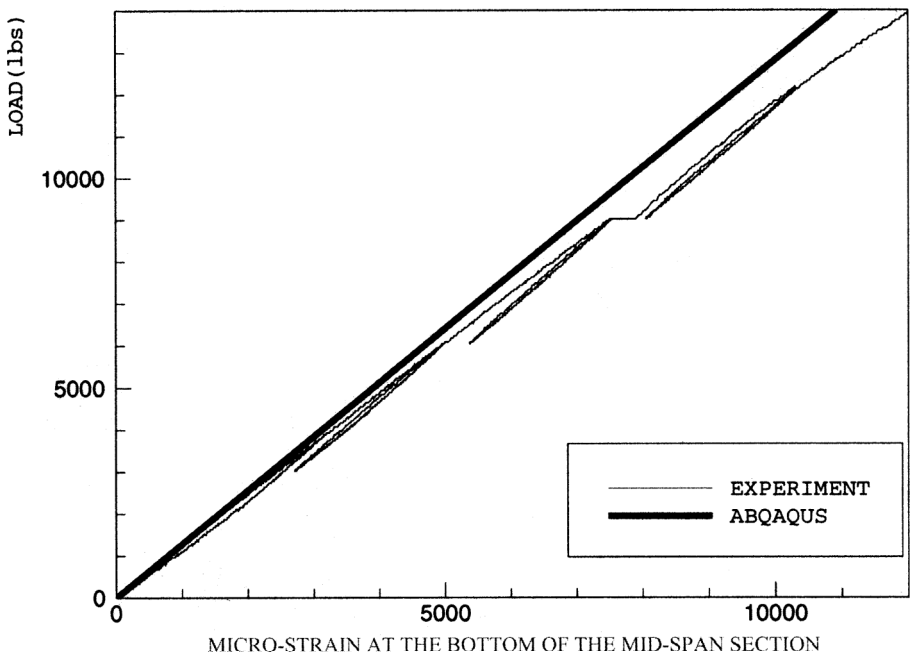

(b) Load *vs.* strain

Note: 1 in = 25.4 mm, 1 lb = 4.45 N

Figure 6. Two-tube assembly bending results.

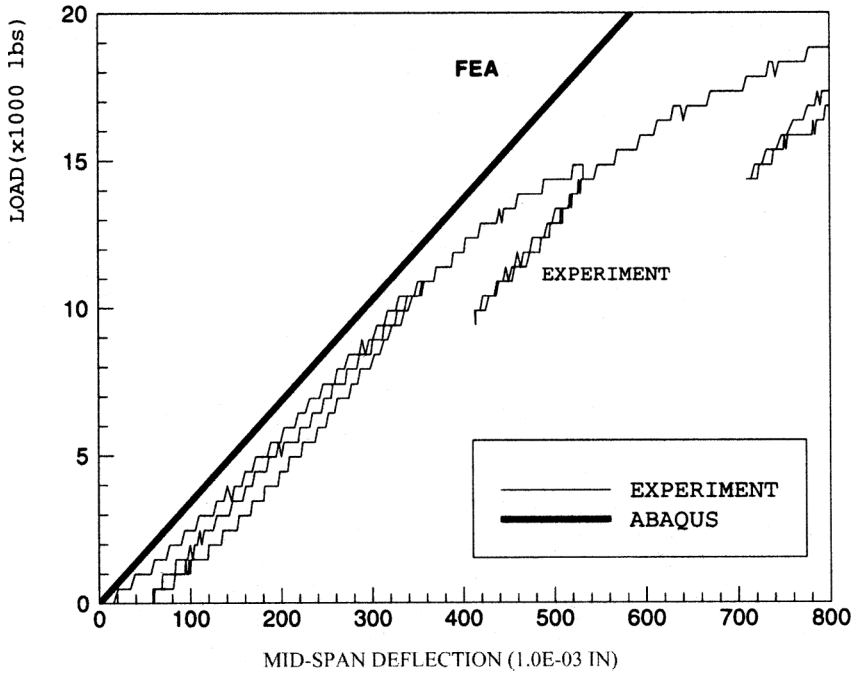

(a) Load *vs.* deflection

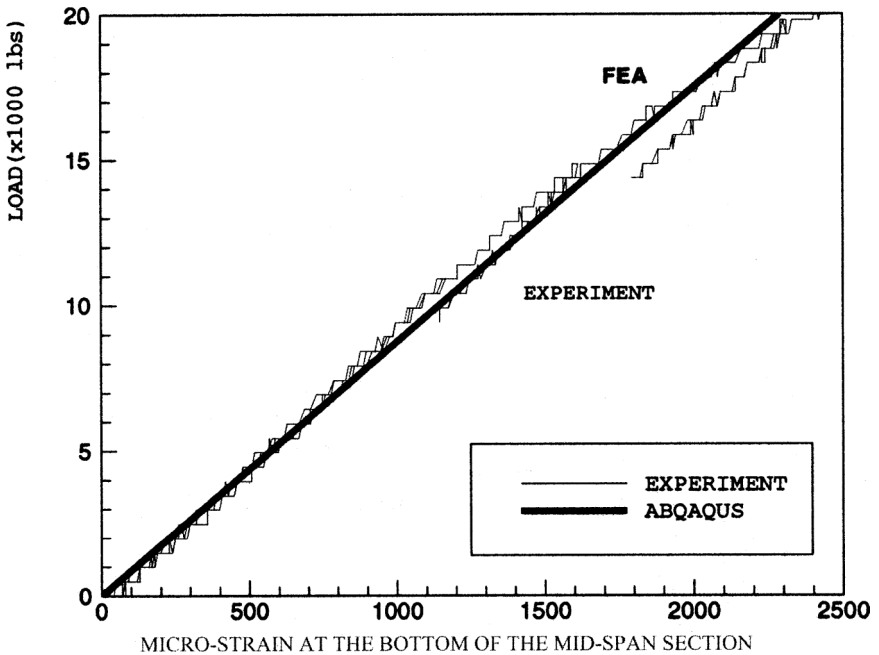

(b) Load *vs.* strain

Note: 1 in = 25.4 mm, 1 lb = 4.45 N

Figure 7. Displacements and strain for four-layer tube assembly.

Table 2.
Comparison of deflection and strain for different shear modulus

	Single tube bending (under 5200 lb)		Four-layer tube assembly bending (under 20 000 lb)	
	Deflection (in)	Micro-strain (in/in)	Deflection (in)	Micro-strain (in/in)
$G_{LM} = 0.6 \times 10^6$ (psi)	5.210	11 310	0.5856	2372
$G_{LM} = 0.06 \times 10^6$ (psi)	6.447	12 570	1.093	2582
Change	23.7%	11.1%	86.6%	8.9%

Note: 1 in = 25.4 mm, 1 lb = 4.45 N, 1 psi = 6894.8 Pa.

square to diamond and the stiffness of the assembly deteriorates until the failure happens at the corners of the third layer tubes (shown in the circle in Fig. 5b). The linear elastic FEA analysis loses significance at the occurrence of the first non-linear event.

Figure 7b is the comparison of the strain measured at the bottom of the mid-span section. When the load exceeds 12 000 lb (53 400 N), the strain still increases linearly and the load *vs*. strain curve (Fig. 7a) remains a straight line even though the deflection is no longer linear. To learn more about this, two additional numerical studies were conducted. They are single tube bending and four-layer tube assembly bending with reduced shear stiffness (G_{LT}) of 60 psi (0.414 GPa), which is 10% of the initial G_{LT}. To reduce the G_{LT} is to simulate the effect of the deteriorated corners of the third layer tubes which reduced the shear stiffness of the structure. The results are listed in Table 2. For the single tube under a load of 5200 lb (23 140 N), the deflection increases 23.7%, while the strain at the bottom of the mid-span section increases 11.1%. For the four-layer tube assembly under a load of 20 000 lb (89 000 N), the deflection increases 86.6%, while the strain at the bottom of the mid-span section increases only 8.9%. It is clear that the deflection is more sensitive to shear stiffness deterioration while the strain at the bottom is less affected. This satisfactorily explains the experimental results in Fig. 7a and b. When the deflection of the four-layer assembly is less than 0.36 in (9.144 mm), the cross-section of the tubes in layer (3) has little change and no failure occurs at the corners. Based on the experimental results and the additional numerical studies of the 4-layer assembly, it is assumed that, for all assemblies reported in this paper, if the ratio of mid-span deflection over the span remains below 0.4% (deflection/span $< 1/250$), the behavior of the assemblies is linear.

Figure 8 shows the normal and shear stress distribution of the four-layer tube assembly under the load of 12 000 lb (53 400 N). Figure 8a is the normal stress along the vertical centerline of the mid-span section (Fig. 5b line A–A). Since shell elements cannot provide the normal stress in the shell thickness direction, in this figure, there is no normal stress along the span direction for the vertical sides of the tubes in layers (1) and (3). Actually, the normal stress in the tube wall normal direction is small and can be ignored. Along Fig. 5b line A–A, the largest tensile stress occurs at the bottom of layer (4). The largest compressive stress appears on

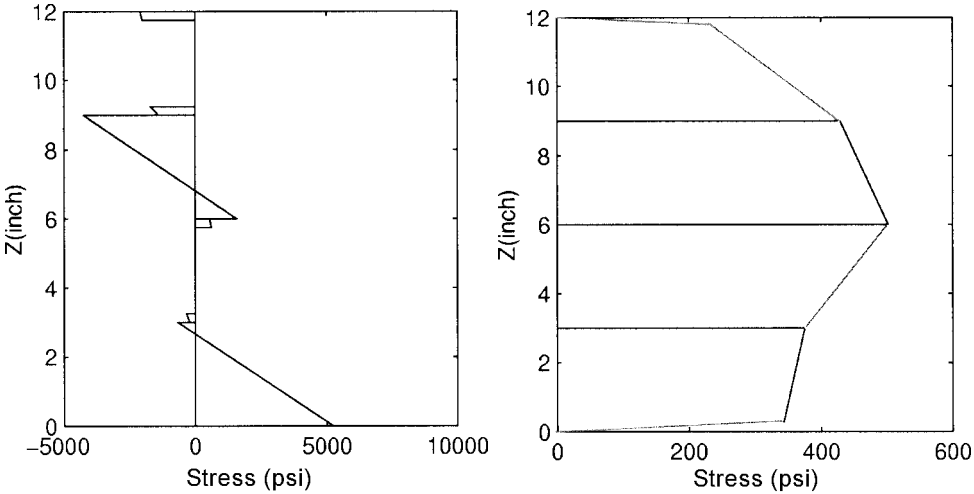

(a) Normal stress through line A (Fig. 5b) (b) Shear stress through line B (Fig. 5b)

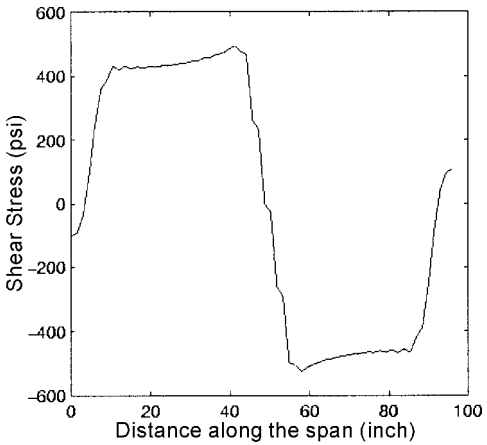

(c) Shear stress in layer 2 along the span

Note: 1 in = 25.4 mm, 1 psi = 6894.8 Pa

Figure 8. Stress distribution for four-layer tube assembly under a load of 12 000 lb (44 500 N).

the top of the tubes in layer (2). This is because the tubes in layer (2) are oriented with fiber direction parallel to the assembly span. The strength requirements can be easily satisfied for layer (2) and layer (4); that is, failure is not controlled by them. Layer (1) is subject to compression failure when the load increases because the tubes are oriented in the transverse direction. Near the loading area, except the tubes in layer (1), tubes experience a stress reverse; i.e. the upper part of the tube is under compression while the lower part is under tension. It is expected that the tubes in layers (3) and (4) should only have tensile stress and the tubes in layers (1) and (2) should only have compressive stress. The cross phenomenon is caused by the composite materials used in the assembly and the complexity of the structure.

When an isotropic elastic material is used, this phenomenon disappears. Away from the loading area, the stress is smaller and its distribution is in agreement with the expectation.

The shear stress distribution along layer (2) in the span direction is shown in Fig. 8c. The largest shear stress occurs near the mid-span (Fig. 5 line B–B). The shear stress distribution at this section along the thickness direction (Fig. 5 line B–B) is shown in Fig. 5b; it reaches its maximum at the top of layer (3). In the experiment, the shear stress does not seem to cause any failure at the glued interface between layers (2) and (3), but it causes a large shear deformation for the tubes in layer (3) when the ratio of deflection over span exceeds 0.4%.

After these case studies, a conclusion can be drawn that the results from ABAQUS for the tube assembly analysis are accurate when the tube assembly behaves as a linear elastic structure. The threshold of linearity is at a ratio of the deflection over span less than 0.4 (deflection/span $< 1/250$).

4. ANALYSIS OF FRP BRIDGE DECK

4.1. FRP tube assembly geometry and applied load

Figure 9 is a FRP bridge deck load model. The deck has a width of W (288 in or 7315 mm) to accommodate two lanes. The height H is 12 in (305 mm). The

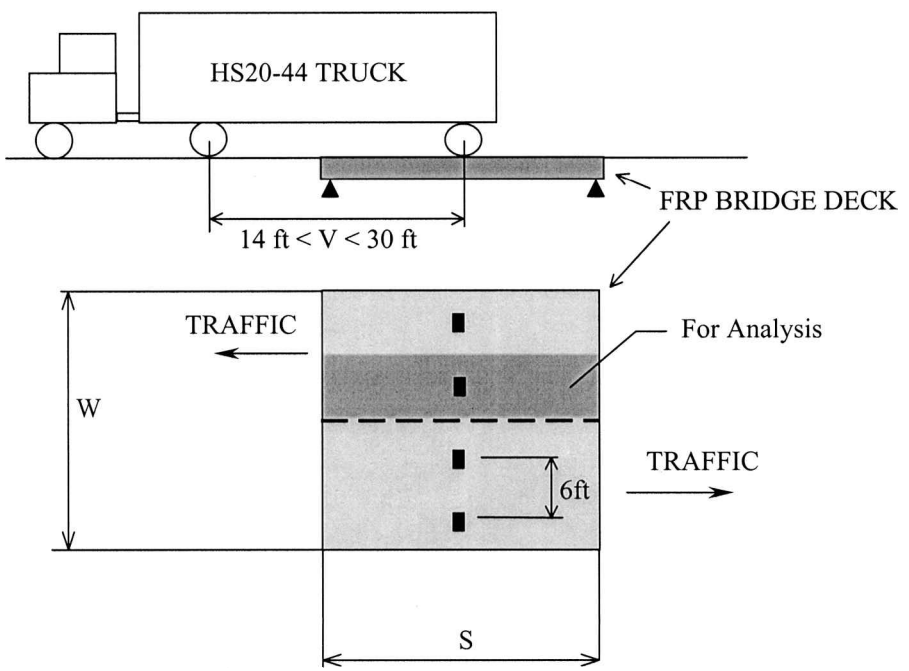

Figure 9. Bridge deck load model. Note: 1 ft = 12 in.

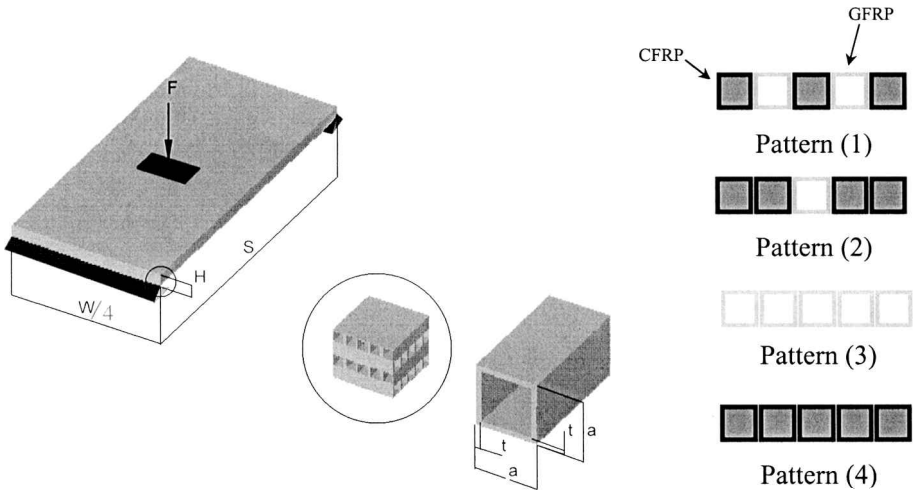

(a) Geometry of bridge deck assembly

(b) Tube layout pattern for layers (2) and (4)

Figure 10. Bridge deck assembly model.

span is chosen from 96 in (2438 mm), 144 in (3658 mm) or 192 in (4877 mm). The assembly has four layers with layer (1) and (3) (counting from top) oriented in the transverse direction and layers (2) and (4) oriented in the width direction. The truck is an HS20-44 standard truck [13]. The severe load condition happens when two wheels are at the mid-span since the specified span, S, is no more than 192 in (4877 mm). The load from each wheel is distributed to an area of 24 in $\times$ 12 in (609.6 mm $\times$ 304.8 mm). A load of 10 000 lb (44 500 N) over each loading area is applied to get the reference deflection and stresses. Under real conditions, the deflection and stresses can be obtained from linearity. For example, if the load is 20 000 lb (89 000 N) for each wheel, the deflection and stresses can be obtained by doubling the deflection and stresses from the reference case. When doing this, the threshold for the linear stage must be satisfied. The ratio of deflection over span must be less than 0.4 (deflection/span $<$ 1/250).

To simplify the ABAQUS model, the deck in Fig. 9 is subdivided into four parts and only one part is analyzed (Fig. 10). By analyzing a quarter portion of the structure with ¼ of the total load at the center, the deflection and stresses for the whole deck under maximum load condition can be obtained with good approximation. The FEA model is shown in Fig. 11. The symmetry in width and span direction of the analyzed part is used.

4.2. Tube size and FRP material

With reference to Fig. 2, the dimensions of the tubes used in this study are: $a = 3$ in (76.2 mm), $t = 0.25$ in (6.35 mm) and $a = 6$ in (152.4 mm), $t = 0.5$ in (12.7 mm).

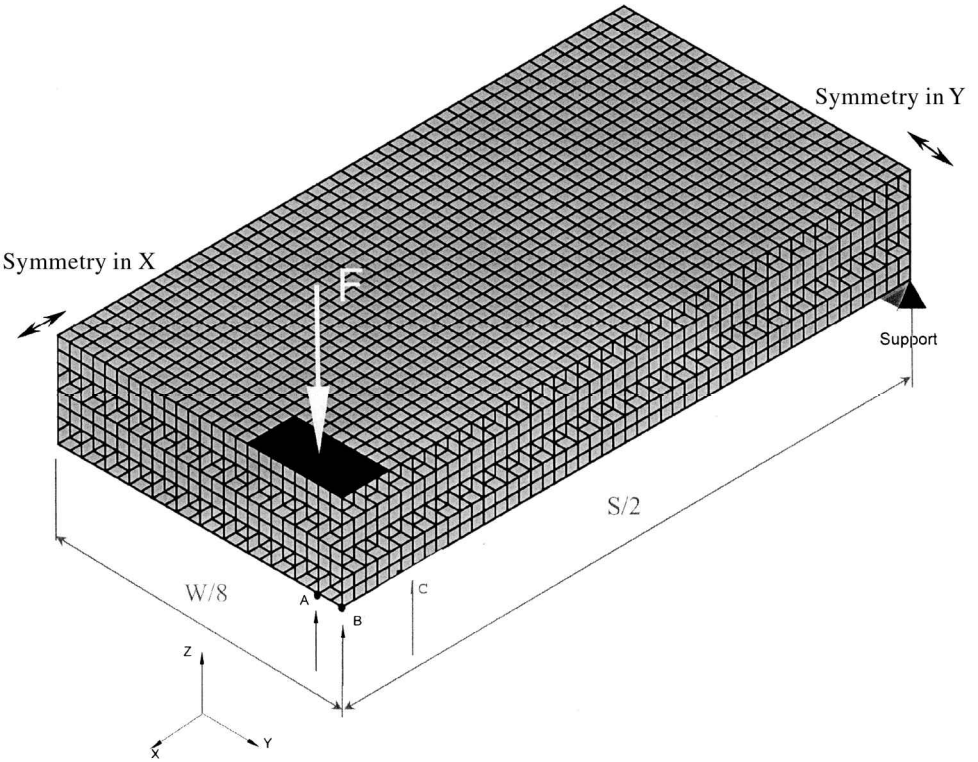

Figure 11. Bridge deck assembly ABAQUS model.

Table 3.
Mechanical properties for GFRP and CFRP used in the assemblies

	E_L (10^6 psi)	E_T (10^6 psi)	G_{LT} (10^6 psi)	ν_{LT}
GFRP	4.35	1.2	0.6	0.26
CFRP	11.05	1.3	1.0	0.3

Note: 1 psi = 6894.8 Pa.

With regards to materials, both GFRP and CFRP are considered. The properties for the GFRP and CFRP tubes used in the assemblies are listed in Table 3.

A four-layer assembly is investigated. Layers (1) and (3) consist of GFRP tubes. The combination of GFRP and CFRP tubes is varied only in layers (2) and (4), where the fiber direction is parallel to the deck span. Four patterns are shown in Fig. 10. Pattern (1) is one CFRP tube by one GFRP tube. Pattern (2) is two CFRP tubes by one GFRP tube. The other two patterns are all GFRP or CFRP.

4.3. Deflection and stress

To obtain meaningful deflection and stresses, it is required that the structure performs in the linear range. A worst case scenario consists of only GFRP tubes

Table 4.
Deflection of tube assemblies under a patch load of 10 000 lb (44 500 N)

Span S (ft)	Width $W/4$ (ft)	Tube size a (in)	Wall thickness t (in)	Boundary condition	Fiber material	Deflection (10^{-3} in)
8	6	3	0.25	simply supported	glass	64.302
					carbon	36.039
					mixed1	47.344
					mixed2	45.131
				clamped	glass	34.735
					carbon	18.997
					mixed1	25.854
					mixed2	24.589
12	6	3	0.25	simply supported	glass	147.7
					carbon	75.909
					mixed1	100.3
					mixed2	95.073
				clamped	glass	68.668
					carbon	38.506
					mixed1	50.835
					mixed2	48.338
		6	0.5	simply supported	glass	36.206
					carbon	20.588
					mixed1	26.805
					mixed2	25.484
				clamped	glass	17.620
					carbon	8.9913
					mixed1	12.234
					mixed2	11.547
16	6	6	0.5	simply supported	glass	61.461
					carbon	34.252
					mixed1	44.376
					mixed2	42.175
				clamped	glass	31.164
					carbon	16.998
					mixed1	22.600
					mixed2	21.403

Note: 1 ft = 12 in, 1 in = 25.4 mm.

with $W = 144$ in (3657 mm), $S = 72$ in (1828 mm), $a = 3$ in (76.2 mm), $t = 0.25$ in (6.35 mm), is chosen to check the requirement, since its ratio of deflection over span is the largest among all the cases discussed herein. The ratio is 0.1477 in/144 in (3.752 mm/3657.5 mm) = 0.1 much less than the threshold 0.4 when the applied load is 10 000 lb (44 500 N). Thus, all the assemblies are assumed to perform in the linear range when the load is less than 40 000 lb (178 000 N).

4.3.1. Deflection. To learn the behavior of the assembly of different configuration, a parametric study is conducted. The assembly varies with three span values; two tube sizes and two thickness values and is subject to simply supported or clamped boundary condition. The deflection for each case is listed in Table 4. For a specific assembly, the deflection from the simply supported boundary condition is about twice the deflection from the clamped boundary condition. This shows that the installation of the assembly has a large effect on its stiffness. The deflection from CFRP tube assembly is half of the deflection from GFRP tube assembly of the same size and boundary condition. When the GFRP tube assembly cannot satisfy the stiffness requirement, a CFRP tube assembly can be considered. When both GFRP and CFRP tubes are used in the assembly, the two mixed patterns give approximately the same deflection, which is much less than using GFRP tubes alone. When the GFRP tube assembly cannot satisfy the stiffness requirement, mixed tube assembly of GFRP and CFRP tubes is an option.

4.3.2. Stress distribution. A typical tube assembly with the mixed (1) pattern is selected to show the stress distribution under a load of 10 000 lb (44 500 N). Figures 12a and b are the tensile and compressive stresses through the thickness of the tube assembly at the mid-span section. Figure 12a is taken from the position shown in Fig. 11, line A. The tubes in layers (2) and (4) at this position are GFRP tubes. The largest tensile stress, 420 psi (2.897 MPa), occurs at the bottom of the mid-span section. The largest compressive stress, 330 psi (2.276 MPa), occurs at the top of the layer (2) tubes. The largest compressive stress in the tubes oriented in width direction, 200 psi (1.379 MPa), occurs at the top of layer (1). Figure 12b is taken from the position shown in Fig. 11, line B. Tubes in layers (2) and (4) at this position are CFRP tubes. The largest tensile stress, 1300 psi (8.966 MPa), happens at the bottom of the assembly in the mid-span. The largest compressive stress, 950 psi (6.552 MPa), occurs at the top of the layer (2) tubes. The maximum stress in CFRP tubes is about three times that of the maximum stress in GFRP tubes in the span direction. This is reasonable since the Young's modulus of CFRP is about three times that of GFRP in the fiber direction.

Along the span direction, the shear stress variation is similar to Fig. 8c. In Fig. 11, line C, shear stress reaches its maximum. Figure 12c is the shear stress through the thickness along this line. The largest shear stress happens at the interface of layer (2) and layer (3) and is 140 psi (0.965 MPa). Shear stress is important when designing the assembly approach. For example, if glue is used to assemble all the tubes together, the glued interface should be tested to see if it is strong enough to withstand the shear stress.

5. FRP BRIDGE DECK DESIGN CONSIDERATIONS

An example is given to show how to use the data in Table 3 when designing a FRP bridge deck. The span of the deck is 144 in (3657 mm). The width is 288 in

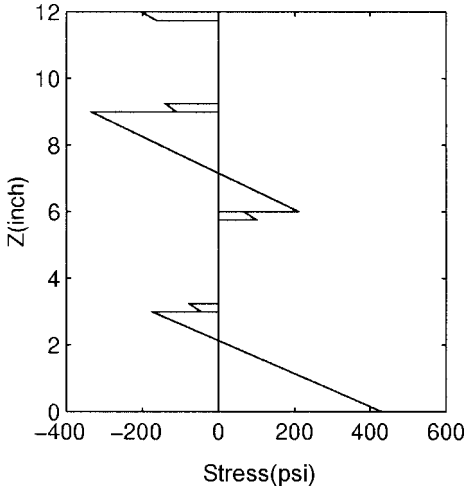

(a) Normal stress through line A

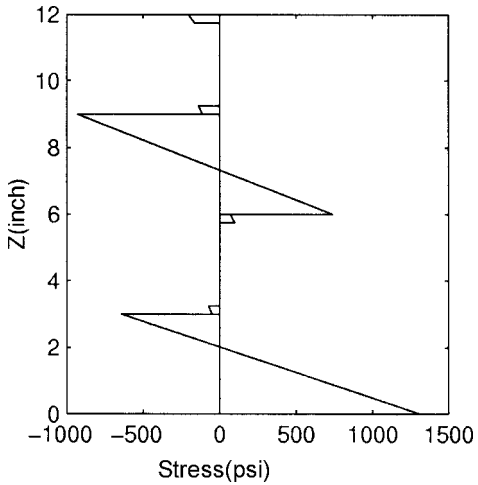

(b) Normal stress through line B

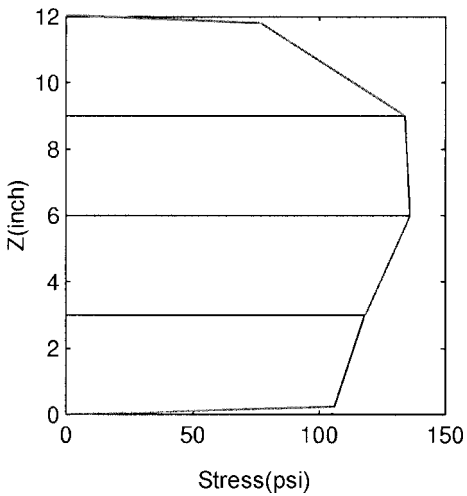

(c) Shear stress through line C

Note: 1 in = 25.4 mm, 1 psi = 6894.8 Pa

Figure 12. Stress distribution for bridge deck assembly.

(7315 mm); thus the deck can hold two lanes. According to AASHTO standards, the possible maximum load for one wheel of an HS20-44 truck is 16 000 lb (71 120 N), with 1.3 as the impact factor; one patch load on the deck is 20 800 lb (92 456 N). If the deck is simply supported, the tube has $a = 3$ in (76.2 mm), $t = 0.25$ in (6.35 mm), the material is GFRP. From the table, deflection for this configuration under the load of 10 000 lb (44 450 N) can be obtained. The deflection is 0.1477 in (3.75 mm). Multiplying 0.1477 by 2.08 (20 800 lb/10 000 lb (92 456 N/44 450 N) = 2.08), the deflection is 0.307 in (7.80 mm). The ratio of deflection over span is 0.21% (0.307 in/144 in (7.80 mm/3657.5 mm) = 0.00213). AASHTO standard

requires that the ratio of deflection over span for highway bridges be less than 1/800 (0.13%). Thus, the deck assembled by GFRP under the simply supported condition cannot satisfy the deflection requirement. If the deck is clamped at both ends, the ratio of deflection over span is 0.1%, which is less than 1/800 (0.13%). If the deck is assembled using both GFRP and CFRP tubes as mixed (1) pattern and is clamped at both ends, the ratio of deflection over span is 0.07%, which is much less than 1/800 (0.13%). Tubes with $a = 6$ in (152.4 mm), $t = 0.5$ in (12.7 mm) can also be used here and the deck will be much stiffer than AASHTO standard requirement.

6. CONCLUSIONS

In this paper, the deflection and stress distribution for FRP tube assemblies of variable size, fiber material, tube wall thickness, and installation are studied. Numerical analysis shows that the strength requirement for FRP composites can be easily satisfied when the FRP assembly is used as a bridge deck. Attention should be paid to the stiffness and interface shear strength requirement. The choice of tube materials for the assembly has a large effect on its stiffness. It is advantageous to use both FEA and experimental method in the designing process.

The numerical work described in this paper was key to selection of the assembly architecture to be used in a demonstration project. Through the interpretation of the experimental results using FEA, it was possible to model and predict the performance of the full-size system under field loads.

Acknowledgements

This work is supported by the Missouri Department of Transportation, National Science Foundation, University Transportation Center and the Navy Center of Excellence for Composites Manufacturing at the Lemay Center for Composites Technology.

REFERENCES

1. F. Seible, US Perspective of Advanced Composites Bridge Technology in Europe and Japan, in: *Proceedings of the Second International Conference on Composites in Infrastructure, ICCI'98*, Tucson, Arizona, USA (1998).
2. A. Zureick, B. Shih and E. Munley, Fiber reinforced polymer bridge decks, *Structural Engineering Review* **7**, 257–266 (1995).
3. T. Ebeido and J. B. Kennedy, Shear and reaction distributions in continuous skew composite bridges, *J. Bridge Engineering* **1**, 155–165 (1996).
4. S. N. Sotiropoulos, H. V. S. GangaRao and A. N. K. Mongi, Theoretical and experimental evaluation of FRP components and systems, *J. Structural Engineering* **120**, 464–485 (1994).
5. S. Youn and S. Chang, Behavior of composite bridge decks subjected to static and fatigue loading, *ACI Structural Journal* **95**, 249–258 (1998).
6. M. E. Mabsout, K. M. Tarhini, G. R. Frederick C. and Tayar, Finite element analysis of steel girder highway bridges, *J. Bridge Engineering* **2**, 83–87 (1997).

7. K. Sennah and J. B. Kennedy, Shear distribution in simply-supported curved composite cellular bridges, *J. Bridge Engineering* **3**, 47–55 (1998).
8. Hibbitt, Karlsson and Sorensen Inc., ABAQUS / Standard User's Manual, Ver. 5.7 (1997).
9. L. C. Bank and P. J. Bednarczyk, A beam theory for thin-walled composite beams, *Compos. Sci. Technol.* **32**, 265–277 (1998).
10. R. Suresh and S. S. Malhotra, Some studies on static analysis of composite thin-walled box beam, *Computers and Structures* **62**, 625–634 (1997).
11. H. J. Patel, A. K. Tripathy and S. Pang, Bending analysis of a laminated composite box beam, in: *Compos. Mater. Technol.*, *ASME PD 53*, pp. 63–71 (1993).
12. P. Kumar, K. Chandrashekhara and A. Nanni, Testing and evaluation of components for a composite bridge deck, *J. Reinf. Plast. Compos.* **20**, 1–21 (2002).
13. American Association of State Highway and Transportation Office (AASHTO), *Standard Specifications for Highway Bridges*, sixteenth edition. Washington D.C. (1996).